The influence of technological defects on the mechanical behavior of CFRP during buckling under compression based on DIC data and acoustic emission

S.V. Slovikov, D.S. Lobanov, E.A. Chebotareva, V.A. Melnikova
Center of Experimental Mechanics, Perm National Research Polytechnic University, Russia
sslovikov@ya.ru, https://orcid.org/0000-0003-3884-3882
cem.lobanov@gmail.com https://orcid.org/0000-0003-1948-436X
cem.chebotareva@mail.ru https://orcid.org/0000-0002-6374-6964
VAMelnikova@pstu.ru https://orcid.org/0000-0002-5163-2054

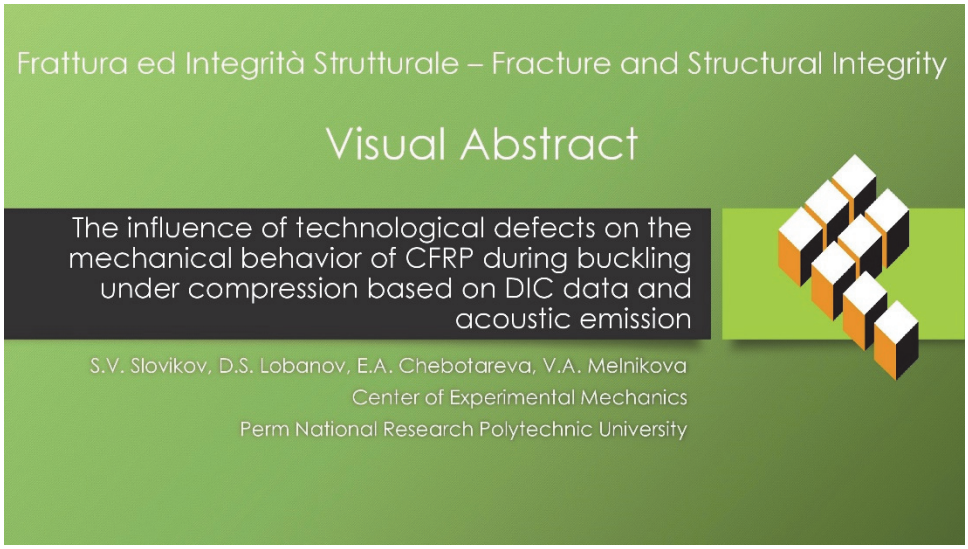

Citation: Slovikov S.V., Lobanov D.S., Chebotareva E.A., Melnikova V.A., The influence of technological defects on the mechanical behavior of CFRP during buckling under compression based on DIC data and acoustic emission, Frattura ed Integrità Strutturale, 69 (2024) 60-70.

Received: 07.03.2024
Accepted: 18.04.2024
Published: 19.04.2024
Issue: 07.2024

KEYWORDS. Carbon-fiber composite, Buckling, Dry-spot, Wrinkles, Mechanical behavior, Compression, Acoustic emission, Digital image correlation.

INTRODUCTION

The capacity to manufacture products with intricate geometries, coupled with the benefits of low mass, high stiffness, and strength, underpins the extensive utilization of polymer matrix composite (PMC) in the aviation sector, especially carbon-fiber-reinforced polymer (CFRP). This domain of application undeniably demands meticulous attention to the fabrication process of the structures. The method for crafting parts from CFRP relies on prepreg technology [1].

In the process of manufacturing using prepreg technology, a range of defects can manifest, including wrinkles, dry-spot, delamination edge, delamination internal, foreign inclusions, fractures, air bubbles/voids, among others [2]. The ASTM E2533-09 "Standard Guide for Nondestructive Testing of Polymer Matrix Composites Used in Aerospace Applications" serves as one of the key regulatory documents defining these defects in PMC [3].

Defects have the potential to significantly diminish both the static and fatigue resistance of a product. Consequently, it is essential to comprehend the influence of the size, geometry, and placement of defects on the mechanical properties of materials [4-7].

Technological defects frequently observed at the fiber-matrix interface encompass adhesion failures, interlaminar delamination, and wrinkles. Meanwhile, matrix-related defects are characterized by the formation of voids and incomplete matrix cure [8-11]. According to the authors, the dry-spot defect is particularly prevalent, arising at various stages of the production process and impacting a broad range of CFRP properties.

The utilization of high-strength carbon fiber composite materials, coupled with the goal to reduce the weight and dimensions of structures, necessitates minimizing the size of the cross sections. Assessing the stability of such thin-walled structures becomes crucial, as their failure typically results from overall buckling or buckling of specific elements [12-14]. This principle applies equally to structures fabricated from CFRP using prepreg technology, where the application of a compressive force exceeding the critical threshold can induce buckling, altering the stress state of the structure as well.

Numerous scientists, including Euler, Engesser, Karman, Timoshenko, Ilyushin, Rabotnov, and others, have shown interest in determining the critical force associated with buckling [15-17].

In the current study, the focus was on plates made of composite material utilizing prepreg technology, characterized by transverse isotropy.

In research addressing the buckling of PMCs, it is highlighted that a shear type of buckling is observed in elastic bodies exhibiting transverse isotropy under compression even with small deformations. Structural elements made of CFRP display lower shear strength relative to their compressive strength [18-20].

For the composite material type being investigated, the shear-induced buckling initially leads to delamination. This phenomenon of accounting for delamination is incorporated into numerous computational studies that consider such mechanical behavior within the finite element model of multilayered composites (laminates) [21-24]. It is crucial to highlight the significance of employing additional monitoring systems when addressing issues related to the examination of strength and deformation characteristics, mechanical behavior, and failure mechanisms of polymer-reinforced composites [25]. Modern experimental mechanics methods, such as the acoustic emission method and the digital image correlation method, are effectively utilized in the experimental investigations of composite materials. Employing these methods enables the acquisition of more precise data regarding the behavior of materials and structures. This, in turn, enhances the processes of design, quality control, and maintenance of these objects [26-30].

In the proposed study, it is suggested to monitor the delamination process using an Acoustic Emission (AE) system. The amplitude-frequency characteristics of the captured acoustic signals enable the identification of specific destruction mechanisms within the spectrum, particularly isolating the delamination process [31].

The aim of the study was to evaluate the impact of internal technological defects on the mechanical performance of CFRP under buckling conditions during compression tests, utilizing data gathered from an acoustic emission signal recording system and digital image correlation.

To meet the study's objectives, the following tasks were established:

- Capturing buckling events through the Vic 3D system;
- Analyzing acoustic emission signals during compression to identify the processes of composite layer separation (delamination) and fiber fracture.

RESEARCH MATERIALS AND METHODOLOGY

For the buckling process to occur, the ratio of the thickness to the height of the material sample under compression must be sufficiently small. In compression tests conducted in accordance with the ASTM D 3410 method on samples made of PMC that meet the thickness requirements of this standard, no buckling is observed [32]. Consequently, the authors conducted tests on carbon fiber samples prepared from plates 2 mm thick. During the fabrication process, simulators of internal technological defects were embedded within the samples.

The study investigates the impact of two specific types of defects: "dry-spot" and "wrinkles". Geometrically, these defects were created in the shapes of a circle with a radius of 10 mm and a square with side lengths of 20 mm, respectively. A

schematic representation of the defects under investigation, along with a diagram detailing the placement of these defects within the carbon fiber samples, is provided in Fig. 1.

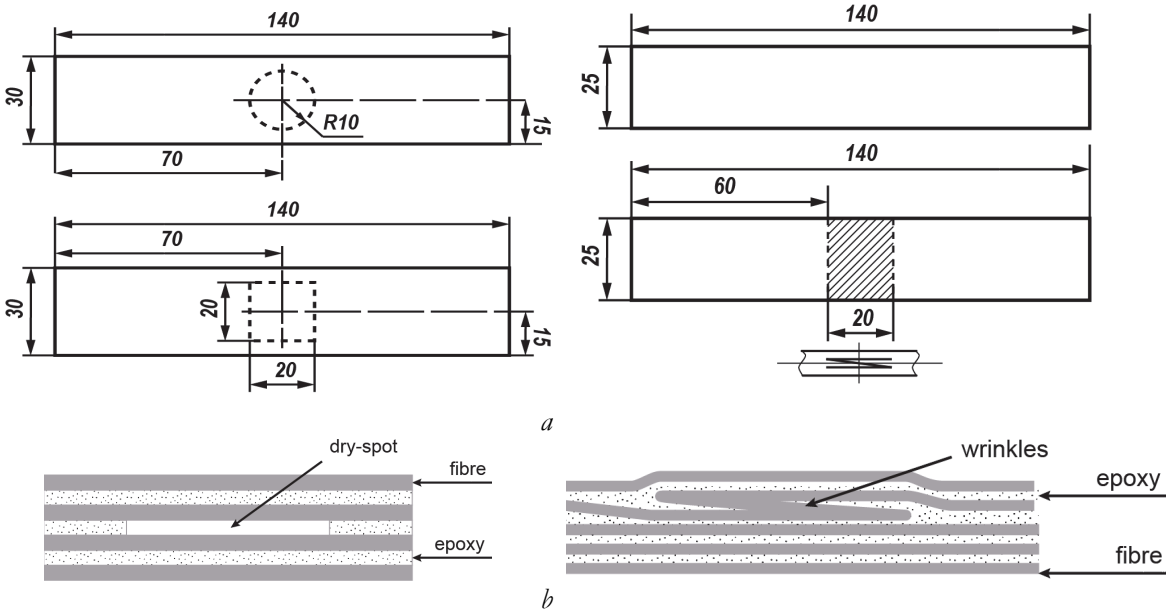

Figure 1: Scheme of samples (*a*) with internal defects (*b*) "dry-spot" and "winkles".

The samples were fabricated using VKU-60 prepreg and VSE1212 polymer matrix with a laying scheme $[0/90]_{10}$, employing standard autoclave molding technology. The thickness of samples was 2.1mm.

The tests were conducted using an Instron 5882 electromechanical system, equipped with precision fixtures designed in accordance with ASTM D 3410 standards. The crosshead speed was set at 1.5 mm/min. Load measurements were performed using a load cell with a capacity of ± 100 kN, and the accuracy of load measurement was maintained at 0.5% of the value measured. The distance maintained between the compression grips was set at 25 mm. In-situ strain and displacement measurements were captured using the Vic-3D digital optical system. During the compression tests, parameters such as maximum stress and elastic modulus were determined. Five samples of each type were tested.

In the compression tests, acoustic emission signals were continuously recorded using the AMSY-6 multichannel system from Vallen Systeme GmbH. A broadband piezoelectric sensor, model AE144A with a frequency range of 100-450 kHz, and a 34 dB preamplifier gain were utilized for signal detection. The data sampling frequency was set at 10 MHz, and the threshold value for AE signal recording was established at 40 dB, to accurately record the applied load, the AMSY-6 system was synchronized with the testing machine through a synchronization unit.

The setup of the equipment, along with the installed device for performing compression tests, is depicted in Fig. 2.

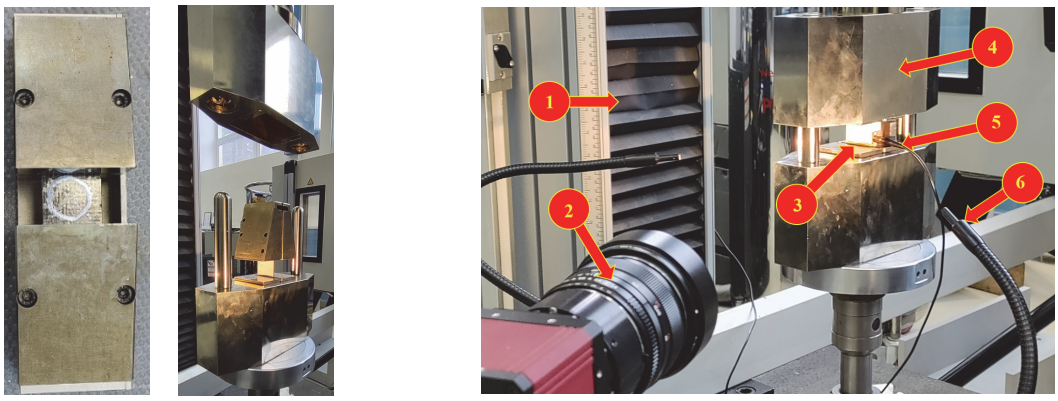

Figure 2: Compression test: *a* - sample in special compression equipment according to ASTM D 3410 before testing; *b* - test progress: 1- Instron 5882 system; 2 –VIC-3D; 3 – carbon fiber sample working area; 4 - compression tooling according to ASTM D 3410; 5 – AE sensor; 6 – additional light source

RESULTS AND DISCUSSION

From the outcomes of the tests, load-displacement and stress-strain diagrams were generated for each specimen and the elastic modulus was determined. The determined values of the elastic modulus and maximum loads achieved during the compression tests are summarized in Tab. 1.

Defect	Elastic modulus, GPa	Maximum load, kN	Maximum stress, MPa	CV, %
without a defect	67.5	15.8	320	4
Dry-spot, a circle	66.3	19.3	320	5
Dry-spot, a square	64.3	18.5	310	5
Wrinkles	68.0	17.7	340	14

Table 1: Sample properties.

All the samples tested experienced failure due to delamination, followed by subsequent buckling, as illustrated in Fig. 3.

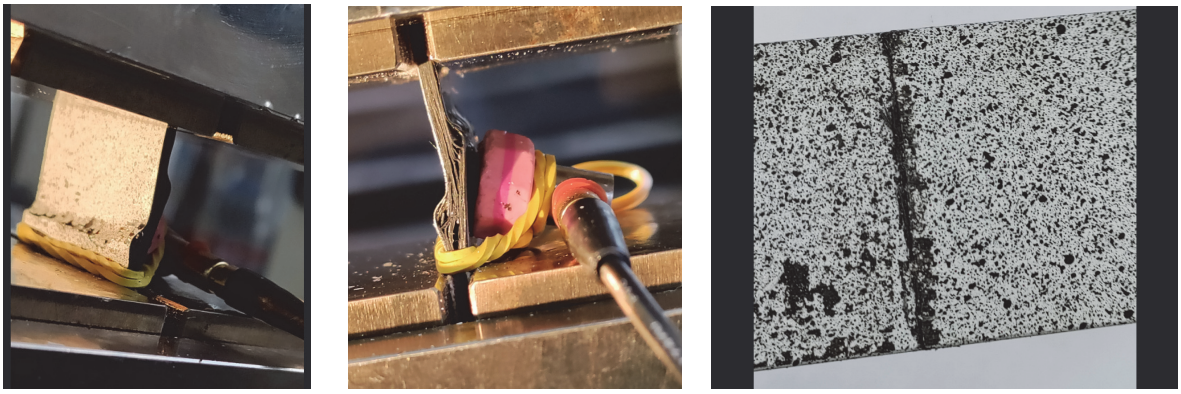

Figure 3: Typical type of specimen failure.

The buckling nature depends on the type of defect and is observed in the attached study by capturing the profiles of transverse displacements in the working area of the samples.
An example of the profiles obtained from the Vic 3D system images is presented in Fig. 4.

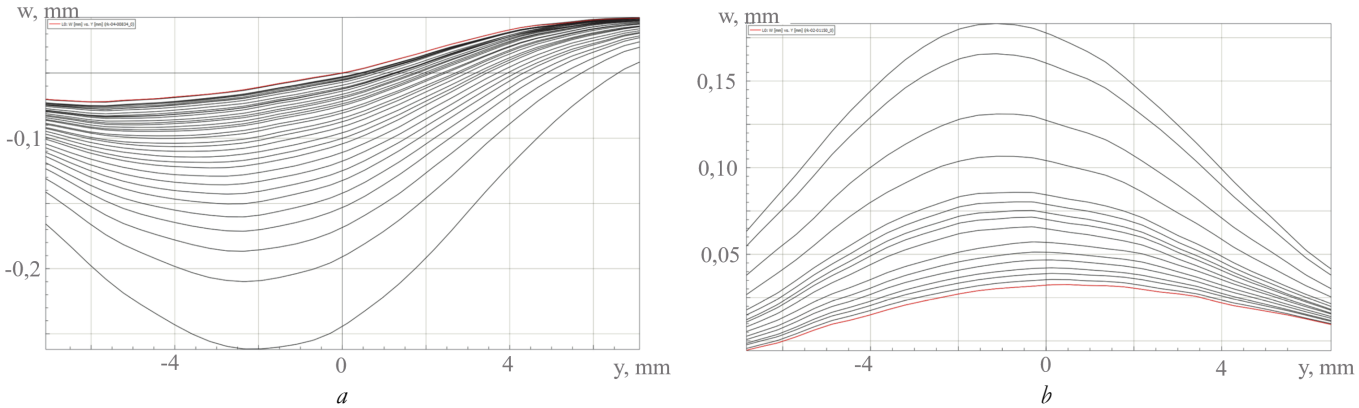

Figure 4: Profiles of the buckling process in the load range from 15 kN (red line) to failure for samples with dry-spot defects: *a* - circle, *b* – square.

From the analysis of the profiles, graphs depicting deflection (w) as a function of the load were derived. Examples of these graphs are shown in Fig. 5.
Under post-critical conditions, the delamination process of CFRP occurs.

In the combined diagrams of AE and the load sensor, it is evident (see Fig. 6) that with the initial delamination, there is an increase in the energy parameter level of AE signals over time preceding the drop in load value. However, in samples with the wrinkles defect, the peak of the energy parameter does not coincide with the maximum load.

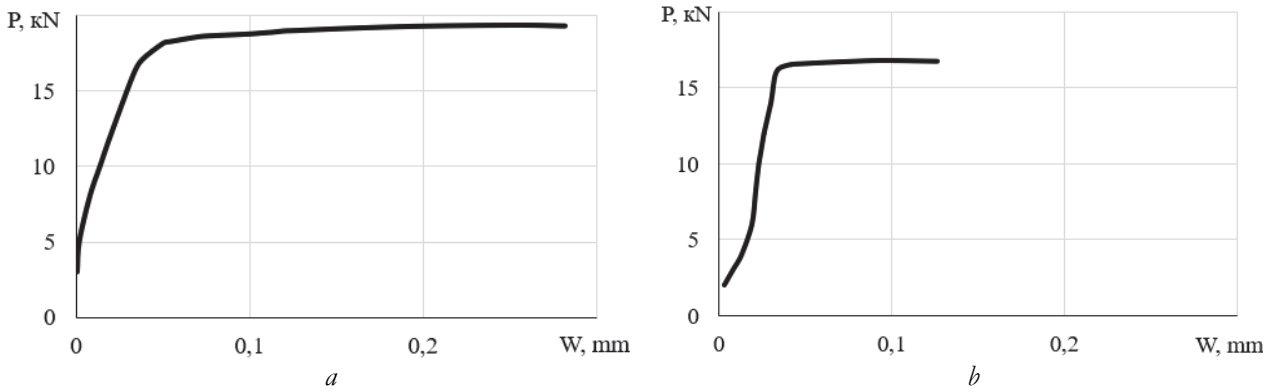

Figure 5: Deflection of the working area of samples with dry-spot defects: *a* - circle, *b* – square.

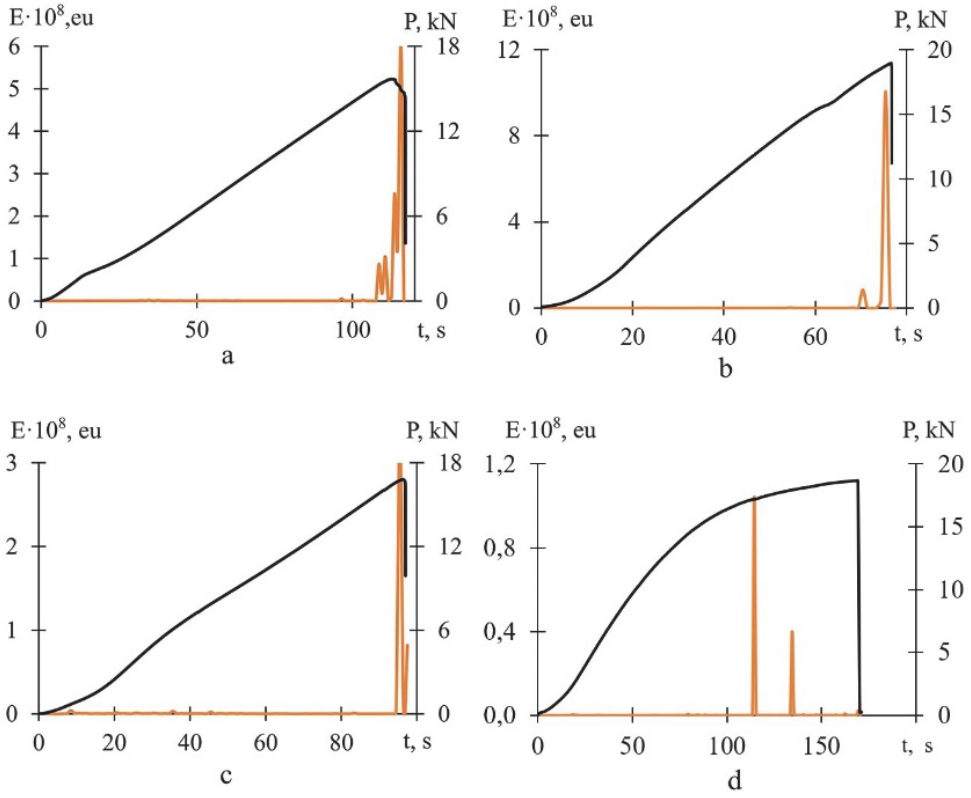

Figure 6: Diagrams of the dependence of the energy parameter of AE signals on time, combined with a graph of loading of samples without defect (a), dry-spot, a circle (b), a square (c) and wrinkles (d).

Throughout the entire test, the energy parameter level of the AE signals remains low. With the onset of fiber breakage, the parameter values increase by several orders of magnitude, and a peak is observed, followed by the sample failure.

Cumulative energy is a parameter that reflects the degree of defect accumulation in the material. To obtain values of cumulative energy, a summation of the energy parameter values for all previous time intervals is conducted. The level of cumulative energy in all samples falls within the same range, with a sharp increase observed upon reaching maximum load (Fig. 7).

Based on the post-processing of AE data, the delamination process, which is not captured by Vic-3D data but is detected through AE signals as a sharp increase in the signal count level, presents significant interest.

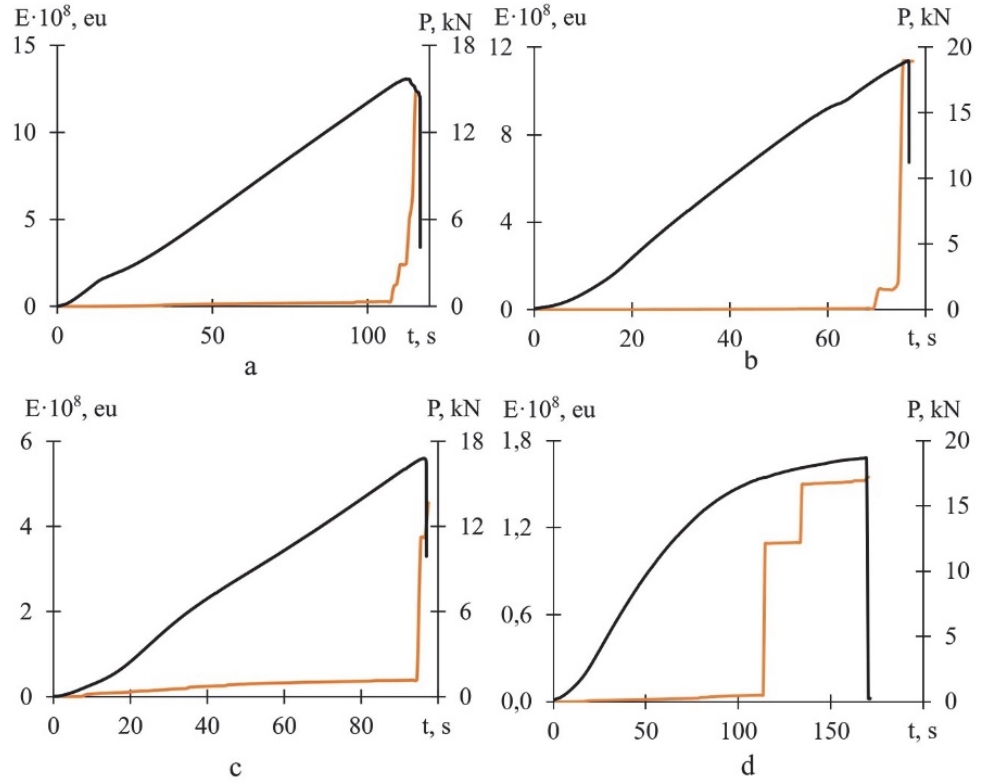

Figure 7: Diagrams of the dependence of the cumulative energy of AE signals on time, combined with a graph of loading of samples without defect (a), dry-spot , a circle (b), a square (c) and wrinkles (d).

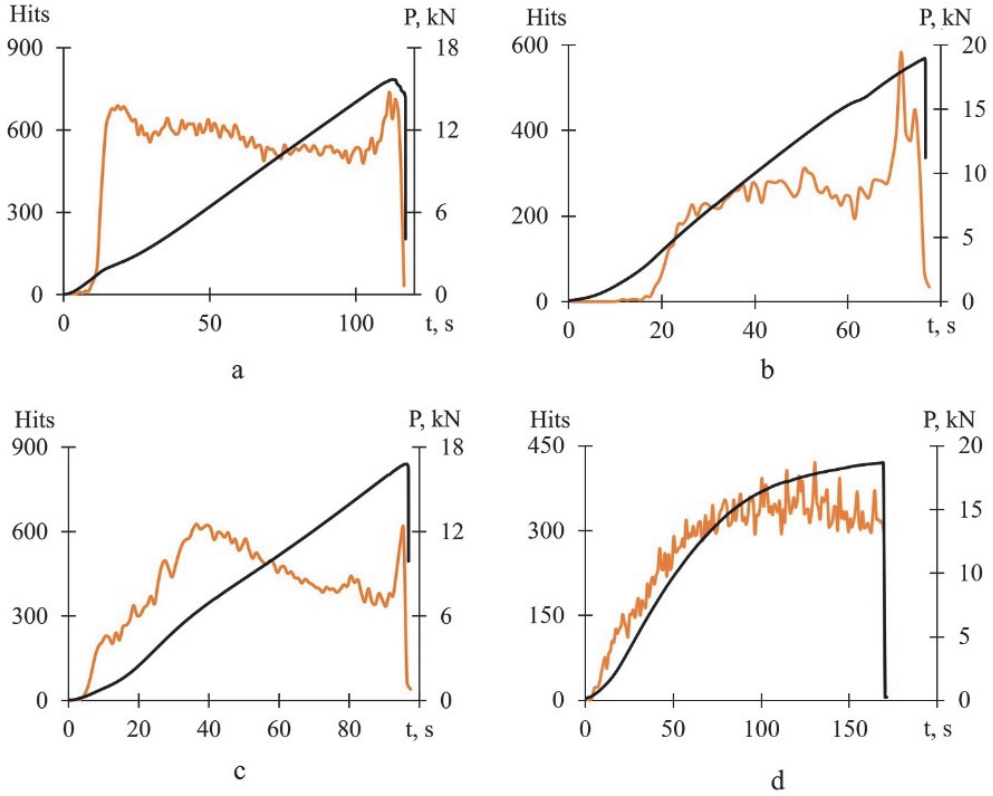

Figure 8: Diagrams of the dependence of the number of AE signals (hits) on time, combined with a graph of loading samples without defect (a), dry-spot , a circle (b), a square (c) and wrinkles (d).

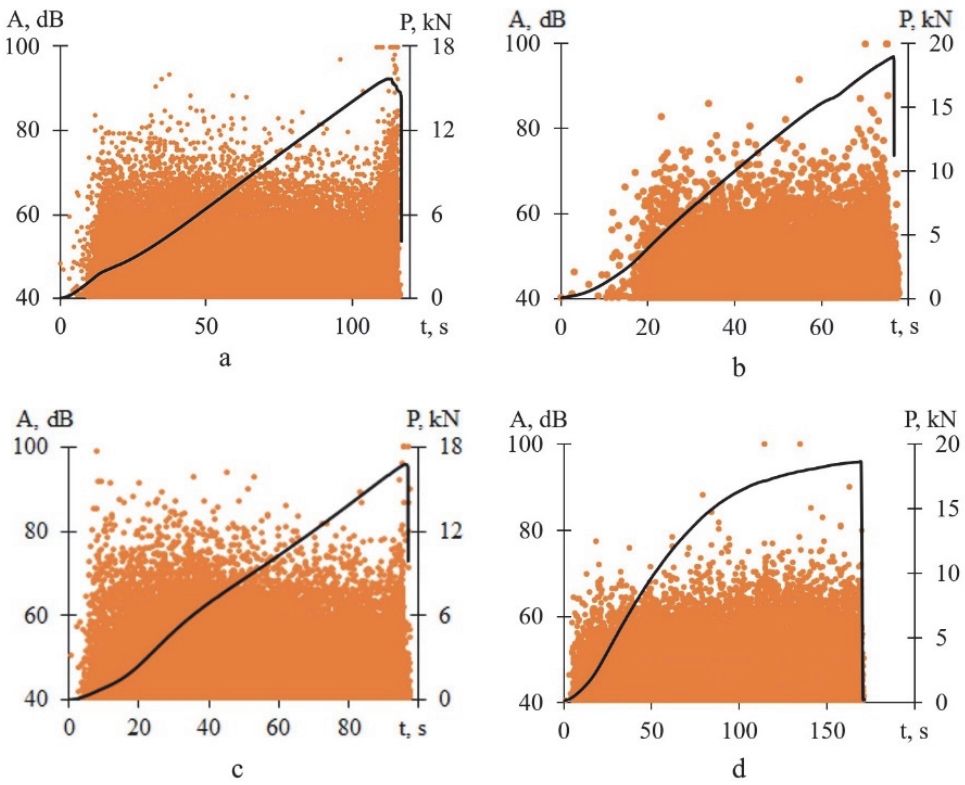

Figure 9: Diagrams of the dependence of peak amplitudes of AE signals on time, combined with a graph of loading samples without defect (a), dry-spot, a circle (b), a square (c) and wrinkles (d).

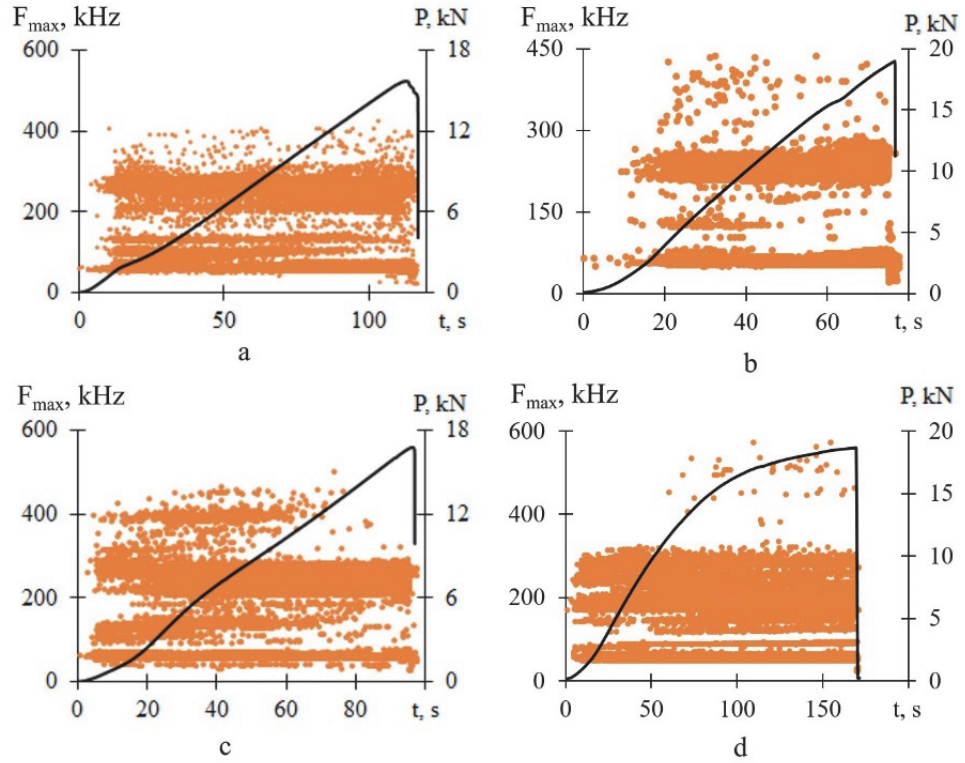

Figure 10: Examples of diagrams of the dependence of peak frequencies of AE signals (F_{max}) on time, combined with a graph of loading samples without defect (a), dry-spot, a circle (b), a square (c) and wrinkles (d).

The signal count level increases at the beginning of the test, then either decreases or remains constant, with the maximum number of signals being recorded upon failure and reaching maximum load. It is noteworthy that for samples without defects, the number of signals stays within the same range throughout the entire test (Fig. 8).
The peak amplitude diagrams (Fig. 9) show that signals seldom reach the maximum amplitude values, with only a few signals of maximum amplitude being recorded towards the end of the test. This may indicate that a failure mechanism such as fiber fracture is almost non-existent in the material. The signals almost immediately reach an amplitude level of 75 dB or more, which does not decrease throughout the duration of the test.
Fig. 10 displays diagrams showing the dependency of the spectral peak frequency (SPF) of AE signals over time, combined with load graphs. Given the sensor's frequency range of 100-500 kHz, only frequencies within this spectrum were analyzed. Based on the data, the signals can be categorized into three frequency ranges. The diagrams reveal that a mid-frequency range predominates in all samples. Moreover, signals within the 200 to 300 kHz range are present throughout the entire test, whereas signals of higher or lower frequencies emerge at the beginning of the test and are almost not recorded after reaching a certain load level. In samples without defects, the mid-frequency range also predominates, but signals across all frequencies were recorded throughout the duration of the test.
The frequency distribution histograms (Fig. 11) confirm the observations made earlier. The number of signals in the mid-frequency range significantly outweighs those in the low and high-frequency ranges. Furthermore, high-frequency signals are fewer by 2-3 orders of magnitude. The presence of low-frequency signals indicates matrix fracture in the material. However, as previously noted, the matrix fracture occurred in the initial stages of loading.

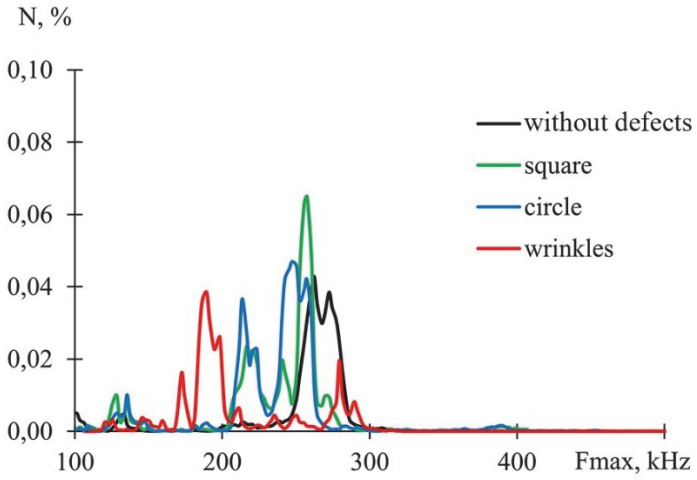

Figure 11: Histograms of the frequency distribution of the spectral maximum

Based on the post-processing of AE and Vic-3D data, the moment of fiber fracture initiation is of interest. This event is not captured by the sensors of the loading system but is detected through AE signals.
In Fig. 12, the evolution of strain fields along the ε_{xx} component on the surface of the samples is depicted, from the moment when the load value (N_1) was 50% lower than the load value corresponding to the onset of fiber fracture (N_2), up to the moment of failure.
Zones with increasing deformation values under loads preceding failure can be observed by analyzing the evolution of deformation fields in the defect area. Notably, these zones are absent in samples without defects. This observation indicates the influence of the studied defect sizes on the mechanical behavior of the material under compressive load.

Conclusions

The experimental study demonstrated that buckling occurs prior to reaching the compressive strength of the CFRP being investigated.
The omission of a single layer of fiber contributes the buckling process, as the critical buckling stress is influenced by the stiffness and shear strength characteristics of the epoxy matrix. Furthermore, the shape of the defect has a significant impact, in that for a round defect, the radii positioned along the direction of compression provide some degree of support compared to a rectangular defect, where the buckling tends to occur slightly earlier.

During compression, acoustic emission data indicate initial delamination due to interlaminar shear within the CFRP. The presence of extra layers in wrinkles results in a stress concentration at the fabric fold, causing transverse shear in the matrix at this location, subsequently leading to its fracture. In this scenario, buckling occurs (under fixed-fixed boundary conditions).

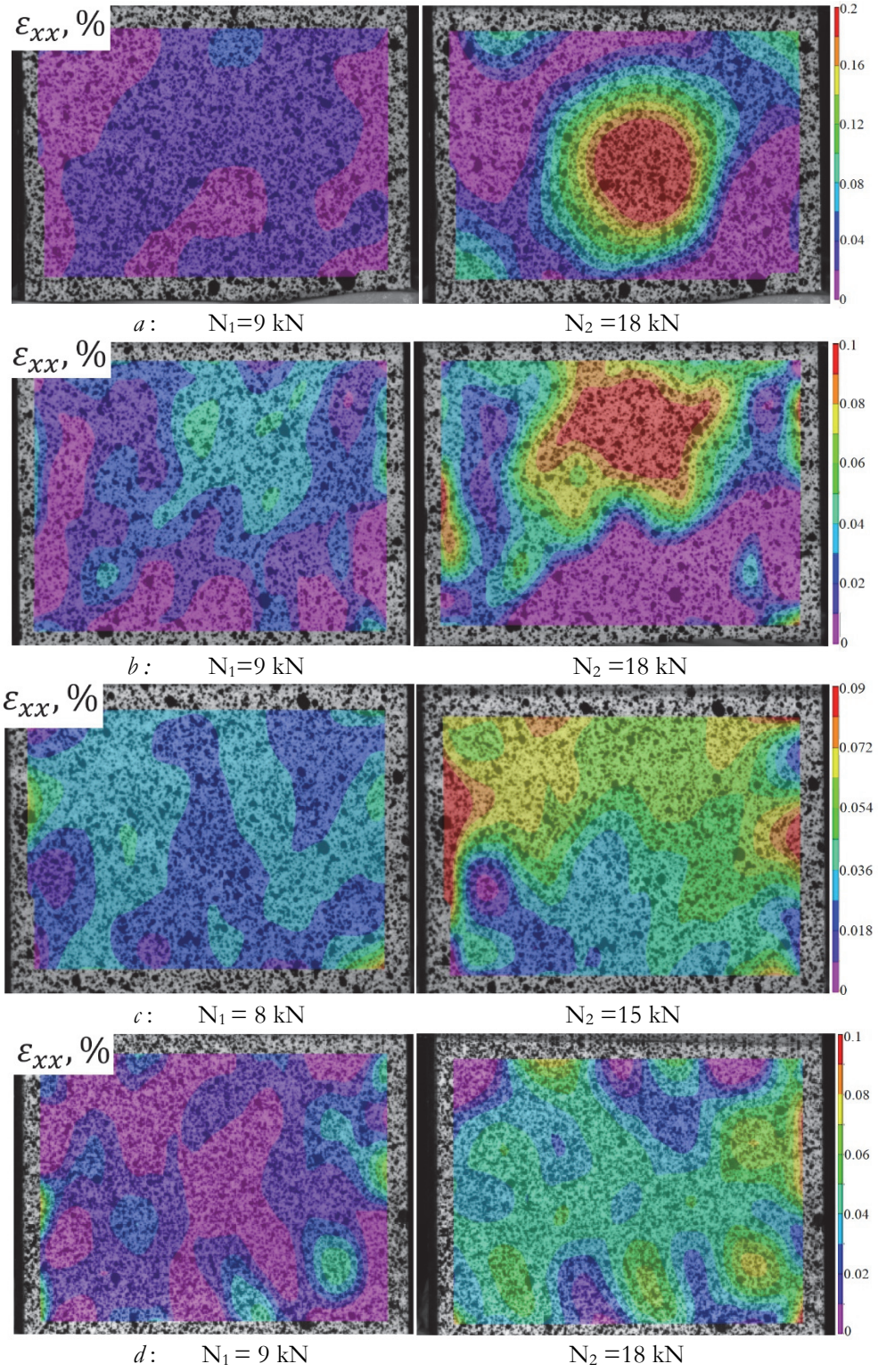

Figure 12: Evolution of deformation fields by component ε_{xx} during delamination processes(N_1, N_2 - levels of compressive load): *a* - dry-spot a circle, *b* – dry-spot a square, *c* - without a defect, *d* – wrinkles.

ACKNOWLEDGEMENTS

This work was carried out with the support of the Russian Science Foundation (Project No 21-79-10205, https://rscf.ru/project/21-79-10205/, accessed on 13 December 2022) at the Perm National Research Polytechnic University.

REFERENCES

[1] Wang, R.-M., Zheng, S.-R., Zheng, Y.-P. (2011). Polymer Matrix Composites and Technology., Polymer Matrix Composites and Technology, Woodhead Publishing, pp. i–iii.
[2] Dikov, I.A., Yakovleva, S.I., Boychuk, A.S., Chertishchev, V. Yu. (2023). Defect classification for 2D fiber-reinforced composites (review), Trudy VIAM, (3(121)), pp. 67–83. DOI: 10.18577/2307-6046-2023-0-3-67-83.
[3] ASTM E2533-09. (2009). ASTM E2533-09 «Standard Guide for Nondestructive Testing of Polymer Matrix Composites Used in Aerospace Applications.
[4] Anoshkin, A.N., Zuiko, V.Y., Tashkinov, M.A., Silberschmidt, V.V. (2015). Repair of damage in aircraft composite sound-absorbing panels, Composite Structures, 120, pp. 153–166. DOI: 10.1016/j.compstruct.2014.10.001.
[5] Armstrong, K.B. (2005). Care and Repair of Advanced Composites, 2nd edition, Warrendale, Pa, SAE International.
[6] Cantwell, W.J., Morton, J. (1992). The significance of damage and defects and their detection in composite materials: A review, The Journal of Strain Analysis for Engineering Design, 27(1), pp. 29–42. DOI: 10.1243/03093247V271029.
[7] Tashkinov, M.A. (2017). Modelling of fracture processes in laminate composite plates with embedded delamination, Frattura ed Integrità Strutturale, 11(39), pp. 248–262. DOI: 10.3221/IGF-ESIS.39.23.
[8] Chertishchev V.Yu. (2020). Development of Technologies and Means of Acoustic Impedance Control of Multilayer Honeycomb Structures from Polymer Composite Materials: thesis, Cand. Sc. (Tech.). Moscow: Bauman MSTU, 180.
[9] Lobanov, D., Slovikov, S., Lunegova, E. (2023). Influence of Internal Technological Defects on the Mechanical Properties of Structural CFRP, Frattura Ed Integrità Strutturale, 17, pp. 74–87. DOI: 10.3221/IGF-ESIS.65.06.
[10] Lobanov, D.S., Strungar, E.M., Zubova, E.M., Wildemann, V.E. (2019). Studying the Development of a Technological Defect in Complex Stressed Construction CFRP Using Digital Image Correlation and Acoustic Emission Methods, Russ J Nondestruct Test, 55(9), pp. 631–638. DOI: 10.1134/S1061830919090031.
[11] Mehdikhani, M., Gorbatikh, L., Verpoest, I., Lomov, S. (2018). Voids in fiber-reinforced polymer composites: A review on their formation, characteristics, and effects on mechanical performance, Journal of Composite Materials, 53, p. 002199831877215. DOI: 10.1177/0021998318772152.
[12] Bazant, Z.P., Cedolin, L. (2010). Stability of Structures: Elastic, Inelastic, Fracture and Damage Theories, World Scientific.
[13] Leipholz, H. (2013). Stability Theory: An Introduction to the Stability of Dynamic Systems and Rigid Bodies, Springer-Verlag.
[14] Yoo, C.H., Lee, S. (2011). Stability of Structures: Principles and Applications, Elsevier.
[15] Polilov, A.N., Rabotnov, Yu.N. (1983). Delamination growth in composites under pressure loading, Izvestiya akademii nauk SSSR. Mehanika twerdogo tela, (4), pp. 166–171.
[16] Prager, W. (1955). The Theory of Plasticity: A Survey of Recent Achievements, Proceedings of the Institution of Mechanical Engineers, 169(1), pp. 41–57.
[17] Timoshenko, S.P., Gere, J.M. (2012). Theory of Elastic Stability, Courier Corporation.
[18] Bai, Y., Keller, T. (2009). Shear Failure of Pultruded Fiber-Reinforced Polymer Composites under Axial Compression, Journal of Composites for Construction, 13(3), pp. 234–242. DOI: 10.1061/(ASCE)CC.1943-5614.0000003.
[19] Staroverov, O., Strungar, E., Wildemann, V. (2021). Evaluation of the survivability of CFRP honeycomb-cored panels in compression after impact tests, Frattura ed Integrità Strutturale, 15(56), pp. 1–15. DOI: 10.3221/IGF-ESIS.56.01.
[20] Wildemann, V.E., Tretyakova, T.V., Strungar, E.M., Tretyakov, M.P. (2018). Deformation and failure of carbon fiber composite specimens with embedded defects during tension-torsion test, Frattura Ed Integrità Strutturale, 12(46), pp. 295–305. DOI: 10.3221/IGF-ESIS.46.27.
[21] Di Sciuva, M., Sorrenti, M. (2019). Bending, free vibration and buckling of functionally graded carbon nanotube-reinforced sandwich plates, using the extended Refined Zigzag Theory, Composite Structures, 227, p. 111324. DOI: 10.1016/j.compstruct.2019.111324.

[22] Kahya, V., University, K.T. (2013). Finite Element Analysis of Laminated Composite Beams under Moving Loads, International Balkans Conference on Challenges of Civil Engineering; 1st International Balkans Conference on Challenges of Civil Engineering.
[23] Kubiak, T., Kolakowski, Z., Swiniarski, J., Urbaniak, M., Gliszczynski, A. (2016). Local buckling and post-buckling of composite channel-section beams – Numerical and experimental investigations, Composites Part B: Engineering, 91, pp. 176–188. DOI: 10.1016/j.compositesb.2016.01.053.
[24] Yuan, F.-G., Miller, R.E. (1990). A higher order finite element for laminated beams, Composite Structures, 14(2), pp. 125–150. DOI: 10.1016/0263-8223(90)90027-C.
[25] Lobanov, D., Yankin, A., Mullahmetov, M., Chebotareva, E., Melnikova, V. (2023). The Analysis of Stress Raisers Affecting the GFRP Strength at Quasi-Static and Cyclic Loads by the Theory of Critical Distances, Digital Image Correlation, and Acoustic Emission, Polymers, 15(9), p. 2087. DOI: 10.3390/polym15092087.
[26] Almeida, R.S.M., Magalhães, M.D., Karim, M.N., Tushtev, K., Rezwan, K. (2023). Identifying damage mechanisms of composites by acoustic emission and supervised machine learning, Materials & Design, 227, p. 111745. DOI: 10.1016/j.matdes.2023.111745.
[27] Bannikov, M., Uvarov, S., Bayandin, Y., Nikitiuk, A., Naimark, O. (2023). Damage-failure transition staging in carbon fiber composite materials under quasistatic and cyclic loading with acoustic and digital image correlation analysis, Procedia Structural Integrity, 47, pp. 685–692. DOI: 10.1016/j.prostr.2023.07.052.
[28] Rubio-González, C., de Urquijo-Ventura, M. del P., Rodríguez-González, J.A. (2023). Damage progression monitoring using self-sensing capability and acoustic emission on glass fiber / epoxy composites and damage classification through principal component analysis, Composites Part B: Engineering, 254, p. 110608. DOI: 10.1016/j.compositesb.2023.110608.
[29] Wang, B., Yang, L., Li, Q., Shu, X., Kang, M. (2024). Mechanical behavior, acoustic emission and principal strain field evolution properties of layered cemented paste backfill under unconfined compression, Construction and Building Materials, 415, p. 135111. DOI: 10.1016/j.conbuildmat.2024.135111.
[30] Wang, M., He, M., Liang, Z., Wu, D., Wang, Y., Qing, X., Wang, Y. (2023). Fatigue damage monitoring of composite laminates based on acoustic emission and digital image correlation techniques, Composite Structures, 321, p. 117239. DOI: 10.1016/j.compstruct.2023.117239.
[31] Lobanov, D.S., Lunegova, E.M. (2023). Evaluation of the Effect of Elevated Temperature and Preliminary Thermal Aging on the Residual Mechanical Properties of a Structural Fiberglass Using the Signals of Acoustic Emission, Mech Compos Mater, 59(1), pp. 101–114. DOI: 10.1007/s11029-023-10084-z.
[32] Slovikov, S., Babushkin, A., Gusina, M. (2023). Nonlinearity of mechanical behavior of 3D-reinforced composites under compression, Frattura Ed Integrità Strutturale, 17(66), pp. 311–321. DOI: 10.3221/IGF-ESIS.66.19.